JOURNAL OF COMPUTATIONAL PHYSICS **136,** 629–639 (1997)
ARTICLE NO. CP975787

On the Numerical Evaluation of Electrostatic Fields in Dense Random Dispersions of Cylinders

Hongwei Cheng* and Leslie Greengard†,[1]

*Department of Civil Engineering and Operations Research, Princeton University, Princeton, New Jersey 08544;
†Courant Institute of Mathematical Sciences, New York University, New York, New York 10012
E-mail: greengard@cims.nyu.edu

Received March 18, 1997

We consider the interface boundary value problem which arises in the evaluation of electrostatic fields in composite materials consisting of dense random dispersions of cylinders in a uniform background. This is a well-studied problem from the viewpoint of homogenization and effective medium theory, but one for which accurate numerical simulations have been difficult to obtain. Size effects, in particular, have been neglected due to the expense of solving the field equation in the presence of large numbers of close-to-touching inclusions. Such features require very fine discretizations, even with the use of adaptive gridding, and cause the linear systems which arise to be highly ill-conditioned. In this paper, we present a new integral equation method for the solution of the interface problem which uses a recently developed method of images to resolve the close-to-touching interactions and the fast multipole method to compute far field interactions. Only minutes of workstation time are needed to solve the field equation with thousands of inclusions, allowing us to carry out large-scale statistical studies of the effective conductivity of random two-phase materials at a variety of volume fractions and contrast ratios.

1. INTRODUCTION

An important area of research in materials science concerns the determination of the effective transport and mechanical properties of composites. There are a variety of theoretical approaches to this problem, including the derivation of rigorous bounds [3, 4, 10, 13, 14, 24, 27, 41, 42], effective medium theory [25, 29, 44], asymptotic approximations [2, 6, 21, 33], Monte Carlo simulations [23], and direct solution of the governing equation [11, 15, 31, 35, 36, 39]. One advantage of the direct solution approach is that the desired properties are obtained with arbitrary precision, controlled only by the accuracy of the numerical method. A second advantage is that, having access to point-wise features of the solution, it is possible to study local field fluctuations, flicker noise, and breakdown phenomena [8].

A variety of numerical methods can be used for direct solution of the field equation, including finite difference and finite element methods, but we will restrict our attention here to methods based on potential theory. The first such method is due to Lord Rayleigh, who considered the problem of conductivity through a regular array of disks or spheres [36]. More recent work using this approach includes [7, 11, 15, 16, 30, 31, 35, 39, 40]. More general integral equation formulations of the interface problem [22, 20] can be used to treat composites with inclusions of arbitrary shape [11, 17], and even anisotropic material properties [15]. While these integral equations result in dense $N \times N$ linear systems, where N is the number of points in the discretization of the interface, fast multipole-accelerated iterative schemes require only $O(N)$ work for the solution process [11, 15, 37]. Despite this methodological advance, however, certain problems have been out of reach. When inclusions are close-to-touching (see Figs. 2 and 6), the number of degrees of freedom required to resolve the solution grows extremely large, and the linear system which has to be solved becomes highly ill-conditioned. Such close encounters occur frequently in large dense dispersions, so that, to date, there are virtually no accurate large-scale numerical simulations of random media at high volume fraction. One exception is the recent work of Helsing [16], who has developed an adaptive fast multipole-accelerated iterative scheme for inclusions of arbitrary shape. It is more general than the approach we outline below, but is significantly more expensive, since we take advantage of detailed analytic features of the problem at hand.

In the present paper, we combine a recently developed method of images [7], which allows us to resolve close-to-touching interactions accurately, with the fast multipole method (FMM) [9, 12, 37], which allows us to compute far field interactions efficiently. The resulting scheme can

[1] The first author was supported by the U.S. Department of Energy under Contract DEFG02-92ER14275. The second author was supported by the Applied Mathematical Sciences Program of the U.S. Department of Energy under Contract DEFG02-88ER25053 and by a NSF Presidential Young Investigator Award.

0021-9991/97 $25.00

compute the electrostatic field in unit cells with thousands of inclusions using only minutes of CPU time on a modern workstation. Using our method, we have tabulated the effective conductivity for a wide range of volume fractions and conductivity ratios and compare our results with Milton's four-point lower bound [28], small system size calculations of Sangani and Yao [40] and Monte Carlo simulation data given by Kim and Torquato [23].

2. THE INTERFACE PROBLEM

Consider a composite material consisting of M randomly distributed disks embedded in a uniform background Ω. If each disk D_i has conductivity σ_i and the background has conductivity σ_0, then the global electrostatic potential u satisfies the partial differential equation,

$$\Delta u = 0 \quad \text{in } \Omega - \bigcup_{j=1}^{M} D_j, \tag{1}$$

$$\Delta u = 0 \quad \text{in } D_j, j = 1, ..., M, \tag{2}$$

$$[u] = 0 \quad \text{on } \bigcup_{j=1}^{N} \partial D_j, \tag{3}$$

$$[\sigma \nabla u] = 0 \quad \text{on } \bigcup_{i=1}^{N} \partial D_i, \tag{4}$$

where $\sigma = \sigma_0$ in $\Omega - \bigcup_{j=1}^{M} D_j$, $\sigma = \sigma_j$ in D_j, and $[f]$ denotes the jump in the quantity f when passing from the interior of D_j to the exterior.

If Ω is the plane $\mathbf{R}^2$, and we wish to determine the response of the material to a uniform applied field, we impose the condition

$$\nabla u(P) \to (1, 0) \quad \text{as } \|P\| \to \infty. \tag{5}$$

If Ω is the unit square, we impose the periodic boundary conditions

$$\begin{aligned} u(x + 1, y) - u(x, y) &= 1, \\ u(x, y + 1) - u(x, y) &= 0. \end{aligned} \tag{6}$$

Let us consider the infinite medium problem first ($\Omega = \mathbf{R}^2$). In order to develop an integral equation formulation, we seek the solution as a single layer potential [19, 20],

$$u(P) = P \cdot (1, 0) + \sum_{j=1}^{N} \int_{\partial D_j} G(P, Q)\rho_j(Q)\, ds_Q, \tag{7}$$

where $\rho_j(Q)$ is an unknown surface charge density and $G(P, Q) = (1/2\pi)\log\|P - Q\|$ is the free-space Green's function. The boundary value problem (1)–(5) can then be shown to be equivalent to the integral equation

$$\begin{aligned} 2\lambda_1 \mathbf{n}_P \cdot (1, 0) &= \rho_1(P) - 2\lambda_1 \sum_{j=1}^{N} \int_{\partial D_j} \frac{\partial G}{\partial n_P}(P, Q)\rho_j(Q)\, ds_Q, \\ &P \in \partial D_1, \\ &\cdots \\ 2\lambda_N \mathbf{n}_P \cdot (1, 0) &= \rho_M(P) - 2\lambda_N \sum_{j=1}^{N} \int_{\partial D_j} \frac{\partial G}{\partial n_P}(P, Q)\rho_j(Q)\, ds_Q, \\ &P \in \partial D_M, \end{aligned} \tag{8}$$

where $\lambda_j = (\sigma_j - \sigma_0)/(\sigma_j + \sigma_0)$, $j = 1, ..., n$, and $\mathbf{n}_P$ is the unit normal vector on the inclusion boundary at position P. To solve (8) numerically, one can discretize $\rho_j(Q)$ on each inclusion boundary in a number of ways, including high-order adaptive refinement [16]. Since the inclusions are disks, however, one can also represent $\rho_j(Q)$ as a Fourier series, which we express in complex notation as

$$\rho_j(Q) = \mathrm{Re}\left(\sum_{k=1}^{\infty} A_j(k) e^{ik\theta}\right). \tag{9}$$

Here, the multipole moments (or Fourier coefficients) $A_j(k)$ are unknown complex numbers and $Q = (x_j + a\cos\theta, y_j + a\sin\theta)$. Since ρ can be shown to be charge neutral, no constant term is needed in the expansion. Substituting the representation (9) into the integral equation (8) yields the infinite-dimensional Rayleigh system

$$\begin{aligned} A_j(k) + \lambda_j \sum_{\substack{m=1 \\ m \neq j}}^{M} \sum_{l=1}^{\infty} \binom{l + k - 1}{k - 1} \left(\frac{a}{z_m - z_j}\right)^{l+k} (-1)^k \overline{A_m(l)} \\ = \begin{cases} 2\lambda_j, & \text{if } k = 1, \\ 0, & \text{if } k > 1, \end{cases} \end{aligned} \tag{10}$$

where $z_j = x_j + iy_j$ is the center of D_j viewed as a point in the complex plane. This method is capable of describing the electrostatic field for any configuration of disks and any prescribed conductivities. In practice, of course, the infinite system (10) must be truncated by ignoring all multipole moments beyond a given order. If the inclusions are reasonably well-separated, then the number of moments required is relatively small and Rayleigh's method gives excellent results. If the inclusions are close-to-touching, however, the charge density ρ can become nearly singular, the number of degrees of freedom grows extremely large and the linear system (10) becomes extremely ill-conditioned.

In order to overcome this problem, we have developed a new integral representation for the interface problem [7], replacing the free-space Green's function $G(x, y)$ with a kernel $K^{\delta}(x, y)$ which incorporates information about nearby disks using the method of images. The construction of this kernel is somewhat complicated and reviewed briefly in the next section.

3. THE METHOD OF IMAGES

Let us first observe that in a dilute suspension, where the spacing between inclusions is far greater than the inclusion radii, the global potential is well approximated by the superposition of single disk solutions

$$u_e(r, \theta) \approx r\cos\theta + \sum_{j=1}^{M} a^2\lambda_j \frac{\cos\theta_j}{r_j}, \tag{11}$$

$$u_j(r, \theta) \approx r\cos\theta + \lambda_j r_j \cos\theta_j, \tag{12}$$

where (r_j, θ_j) are the coordinates of the point (r, θ) with respect to the jth disk center. Using complex notation, we can write this as

$$u_e(z) \approx \mathrm{Re}\left(z + \sum_{j=1}^{M} \frac{a^2\lambda_j}{z - z_j}\right),$$

$$u_j(z) \approx \mathrm{Re}(z + \lambda_j(z - z_j)),$$

where z_j is the center of the jth disk.

As the inclusions approach one another, however, the disks interact more and more strongly. Rather than include higher and higher order multipole corrections as in Rayleigh's method, the method of images [18, 26, 32, 33] proceeds by representing the solution in terms of a series of dipole fields. A precise statement of this result is given in the following lemma, whose proof can be found in [7].

LEMMA 3.1. *Let D_1 and D_2 be nonintersecting disks of radius a centered at z_1 and z_2 with identical conductivities σ_d, and let the background medium have conductivity σ_0 (Fig. 1). Then, in the presence of a uniform applied field* (1, 0), *the potential is given by*

$$u_e = \mathrm{Re}\left(z + \sum_{k=1}^{\infty} \frac{\alpha_1^{(k)}}{z - z_1(k)} + \sum_{k=1}^{\infty} \frac{\alpha_2^{(k)}}{z - z_2(k)}\right)$$

$$u_1 = \mathrm{Re}\left(z + \lambda(z - z_1) + (1 - \lambda)\sum_{k=1}^{\infty} \frac{\alpha_2^{(k)}}{z - z_2(k)}\right) \tag{13}$$

$$u_2 = \mathrm{Re}\left(z + \lambda(z - z_2) + (1 - \lambda)\sum_{k=1}^{\infty} \frac{\alpha_1^{(k)}}{z - z_1(k)}\right),$$

where

$$\lambda = \frac{\sigma_d - \sigma_0}{\sigma_d + \sigma_0}, \quad \alpha_1^{(1)} = a^2\lambda, \quad a_2^{(1)} = a^2\lambda,$$

$$z_1(1) = z_1, \quad z_2(1) = z_2,$$

and for $k > 1$

$$z_1(k) = z_1 + a^2/(\overline{z_2(k-1) - z_1})$$

$$z_2(k) = z_2 + a^2/(\overline{z_1(k-1) - z_2}) \tag{14}$$

$$\alpha_1^{(k)} = a^2 \cdot \overline{\alpha_2^{(k-1)}/(z_1(k-1) - z_2)^2}$$

$$\alpha_2^{(k)} = a^2 \cdot \overline{\alpha_1^{(k-1)}/(z_2(k-1) - z_1)^2}. \tag{15}$$

The limiting image points are given by

$$z_1(\infty) = \frac{z_1 + z_2}{2} - \sqrt{ad + d^2/4} \cdot \frac{z_2 - z_1}{|z_2 - z_1|},$$

$$z_2(\infty) = \frac{z_1 + z_2}{2} + \sqrt{ad + d^2/4} \cdot \frac{z_2 - z_1}{|z_2 - z_1|}, \tag{16}$$

where $d = |z_2 - z_1| - 2a$ is the distance between the two disks.

It is important to note that Rayleigh's method and the method of images are both integral equation methods. For the two disk problem, the former is based on seeking the global potential u in the form of a single layer potential,

$$u(P) = x + \sum_{j=1}^{2} \int_{\partial D_j} G(P, Q)\rho_j(Q)\, ds, \tag{17}$$

where $G(P, Q)$ is the free-space Green's function and ρ is the charge density. In this case, the kernel $G(P, Q)$ is simple to evaluate, but ρ becomes very complex if the disks are closely spaced, requiring many Fourier modes to resolve. The method of images is based on the integral representation

$$u(P) = x + \sum_{j=1}^{2} \int_{\partial D_j} K(P, Q)\mu_j(Q)\, ds, \tag{18}$$

where $K(P, Q)$ incorporates the influence of all images according to Eq. (13). Inserting the integral representation (18) into the system (8), with $\partial G/\partial n$ replaced by $\partial K/\partial n$, yields the analytic solution

$$\mu_j(Q) = 2\lambda_j \cos\theta, \tag{19}$$

where $Q = (x_j + a\cos\theta, y_j + a\sin\theta)$. By sacrificing simplicity of the kernel, the integral equation can be inverted analytically and the solution μ_j resolved with only one Fourier mode.

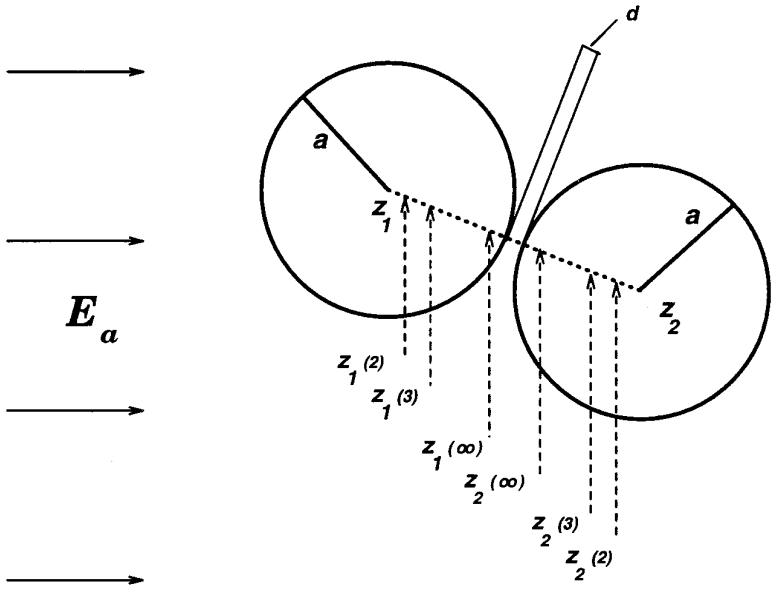

FIG. 1. Two disks separated by a distance d.

Unfortunately, the multidisk case is not so simple. To see this, suppose that we compute the image series generated by each pair of disks using Lemma 3.1, which we refer to as *first-order reflections.* These images must then themselves be reflected into all other disks, generating *second-order reflections*, and so on. The total number of reflections required grows dramatically with the number of disks, rendering the method of images impractical for large-scale problems.

In our earlier work [7], we decided to investigate the behavior of a method which is situated somewhere between the Rayleigh approach and the construction of the exact solution using images. An extremely effective method is obtained from the integral representation

$$u(P) = x + \sum_{j=1}^{M} \int_{\partial D_j} K_j^{\delta}(P, Q)\mu_j(Q)\, ds, \tag{20}$$

where $K_j^{\delta}(P, Q)$ includes the influence of all first-order reflections generated by interactions with disks which lie within a distance δ of D_j. In practice, we choose $\delta = a$, where a is the disk radius. Thus, in the absence of nearby disks, $K_j^{\delta}(P, Q)$ is just the free space kernel.

There is, however, an analytical obstacle to using this idea: the densities μ_j will no longer be pure dipole distributions and the formulae of Lemma 3.1 do not apply. On the other hand, each μ_j is still a charge distribution on ∂D_j whose far field can be expressed as a multipole expansion. The following theorem, taken from [7], gives a simple formula for reflecting a multipole expansion of arbitrary order.

THEOREM 3.1. *Suppose that D_1 is a disk of radius a, centered at z_1 with conductivity σ_1, embedded in the infinite medium* **C** *of conductivity σ_0. Suppose also that $\lambda = (\sigma_1 - \sigma_0)/(\sigma_1 + \sigma_0)$ and that Φ is a multipole source centered at z_2 with $|z_1 - z_2| > a$,*

$$\Phi(z) = \sum_{k=1}^{p} \frac{\alpha(k)}{(z - z_2)^k}.$$

Let $z_I = z_1 + a^2/(\overline{z_2} - \overline{z_1})$ and let

$$\Phi_I(z) = \sum_{k=0}^{p} \frac{\beta(k)}{(z - z_I)^k},$$

where $\overline{\beta(k)}$ (the conjugate of $\beta(k)$) satisfies

$$\overline{\beta(k)} = -\lambda \left(\frac{a^2}{z_2 - z_1}\right)^k \sum_{m=k}^{p} \binom{m}{k} \left(\frac{-1}{z_2 - z_1}\right)^m \alpha(m) \tag{21}$$

for $k = 0, 1, \ldots, p$. Then the functions

$$u_0 = \mathrm{Re}(\Phi(z) + \Phi_I(z)),$$
$$u_1 = \mathrm{Re}((1 - \lambda)\Phi(z))$$

are harmonic in $\mathbf{C} - (D_1 \cup z_2)$ *and* D_1, *respectively, and satisfy the interface conditions*

$$u_0 = u_1 \qquad \text{on } \partial D_1,$$
$$\sigma_0 \frac{\partial u_0}{\partial n} = \sigma_1 \frac{\partial u_1}{\partial n} \quad \text{on } \partial D_1.$$

If we now expand the charge density μ_j on disk D_j as a Fourier series,

$$\mu_j(Q) = \mathrm{Re}\left(\sum_{k=1}^{p} \hat{\mu}_j(k) e^{ik\theta}\right),$$

where $Q = (x_j + a\cos\theta, y_j + a\sin\theta)$, then the far field induced by μ_j is given by the multipole expansion of degree p,

$$\Phi_j(z) = \mathrm{Re}\left(\sum_{k=1}^{p} \frac{\alpha_j(k)}{(z - z_j)^k}\right),$$

where

$$\alpha_j(k) = -\frac{a^{k+1}\overline{\hat{\mu}_j(k)}}{2k}.$$

The first-order reflections in the integral representation (20) for u are image series like (13), but where the reflections are obtained according to formula (21).

Unlike the pure method of images, however, the coefficients $\mu_j(k)$ are now unknown, and we must solve a linear system to obtain them. Imposing the flux interface condition (4), we obtain

$$2\lambda_1 n_1(P) = \mu_1(P) - 2\lambda_1 \sum_{j=1}^{M} \int_{\partial D_j} \frac{\partial K_j^\delta}{\partial n}(P, Q)\mu_j(Q)\, ds, \qquad P \in \partial D_1,$$
$$\cdots \tag{22}$$
$$2\lambda_M n_1(P) = \mu_M(P) - 2\lambda_M \sum_{j=1}^{M} \int_{\partial D_j} \frac{\partial K_j^\delta}{\partial n}(P, Q)\mu_j(Q)\, ds, \qquad P \in \partial D_M,$$

where $\lambda_j = (\sigma_j - \sigma_0)/(\sigma_j + \sigma_0)$, and $n_1(P)$ denotes the x-component of the unit outward normal at P. The actual unknowns in this system are the Fourier modes $\hat{\mu}_j(k)$, but writing the fully discrete linear system is not particularly informative. More critical are the determination of how many Fourier modes p are required and how many reflections in the image series need to be carried out to achieve a specified precision. These questions are answered in detail in [7], and we simply summarize the results here:

1. In a random dispersion of disks, *independent of their spacing*, the error in truncating each multipole expansion after p terms is of the order

$$E_p = O(0.7^p). \tag{23}$$

2. If two disks are separated by a distance d and a precision ε is desired, then the number of reflections required is of the order $O(\log(d\varepsilon)/2\log(1 - \sqrt{d}))$.

3. Let D_1 be a disk of radius a centered at z_1 and let

$$\alpha^{(m)}(k)/(z - z_2(m))^k$$

be a reflected multipole source, where $z_2(m)$ is defined in Eq. (14). Suppose that

$$|\alpha^{(m)}(k)| < \frac{\delta^{k+1}}{k\lambda}\varepsilon, \tag{24}$$

where $\delta = |z_1 - z_2(m)| - a > 0$. Then subsequent reflections of the kth order multipole moment can be ignored with an error bounded by ε. This result provides a dynamic criterion for halting the reflection process.

4. FAST MULTIPOLE ACCELERATION

Having settled the question of how to handle the nearly singular interactions among closely spaced disks by construction of the kernel $K^\delta(P, Q)$, it remains to actually solve the discrete version of the integral equation (22) efficiently. For this we use the iterative method GMRES [38]. For a system with M inclusions, direct calculation of the necessary matrix–vector product requires $O(M^2)$ work, not because of the image computations, but as a result of the *long-range* interactions. Over the last decade, a number of fast algorithms have been developed which compute long-range Coulomb interactions efficiently, and we have chosen to incorporate one of these, namely the *fast multipole method* (FMM), into our scheme. With this, the cost of the matrix–vector product is of the order $O(M)$. We refer the reader to the original papers [9, 12, 37] for a detailed discussion of the method and to the papers [11, 16] for examples of its incorporation into the standard integral equation approach based on the integral equation (8).

Remark 4.1. The only nonstandard feature of the FMM implementation here is the following: as first-order reflections of a given disk D_k are generated in the calculation of near-neighbor interactions, the image multipole expan-

sions must be included in the far-field representation of the disk D_k in order for the representation to be self-consistent.

4.1. *Periodic Boundary Conditions*

In order to compute effective transport properties of bulk materials, we need to impose the periodic boundary conditions (6). For this, we solve the equation

$$\begin{aligned} 2\lambda_1 n_1(P) &= \mu_1(P) - 2\lambda_1 \sum_{j=1}^{M} \int_{\partial D_j} \frac{\partial K_j^\delta}{\partial n}(P, Q)\mu_j(Q)\, ds, \\ &\qquad P \in \partial D_1, \\ &\cdots \\ 2\lambda_M n_1(P) &= \mu_M(P) - 2\lambda_M \sum_{j=1}^{M} \int_{\partial D_j} \frac{\partial K_j^\delta}{\partial n}(P, Q)\mu_j(Q)\, ds, \\ &\qquad P \in \partial D_M, \end{aligned} \tag{25}$$

where K_j^δ is the doubly periodic Green's function, modified to include the influence of all first-order reflections generated by interactions with disks (including periodic images) which lie within a distance δ of D_j. The fast multipole method allows for the computation of the doubly periodic Green's function at essentially the same cost as the infinite medium problem [12].

Once the integral equation is solved, the effective conductivity can be obtained from the net dipole moment D induced by the charge distributions on each disk, as well as all of their images, from the standard formula [11, 16]

$$\sigma_{eff} = \sigma_0(1 + D).$$

5. NUMERICAL RESULTS

In this section, we evaluate the performance of the method described above, which has been implemented in FORTRAN 77. Although we can evaluate the electric field at any location, we will focus our attention on a single functional of the field, namely the effective conductivity. We are primarily interested in studying the behavior of the effective conductivity as we vary the volume fraction, conductivity ratio, and system size (the number of distinct disks per unit cell). Except for the last example, all disk configurations were generated by a Monte Carlo procedure [10, 34]. For this, we begin by placing all disks at the lattice sites of a regular square or hexagonal array. Each disk is then given a small tentative displacement in a random direction. The move is accepted or rejected according to whether or not the new position will cause the disk to overlap with its neighbors. One simulation sweep consists of trying to move each disk once and the length of the displacement is chosen so that the probability of acceptance is approximately 50%. This process is repeated many times until an equilibrium state is achieved. For a system with 100 disks, 200 simulation sweeps can be shown to be sufficient (Kim and Torquato [23]) for volume fractions in the range [0, 0.7]. The random configurations we use in our examples were generated using thousands of simulation sweeps.

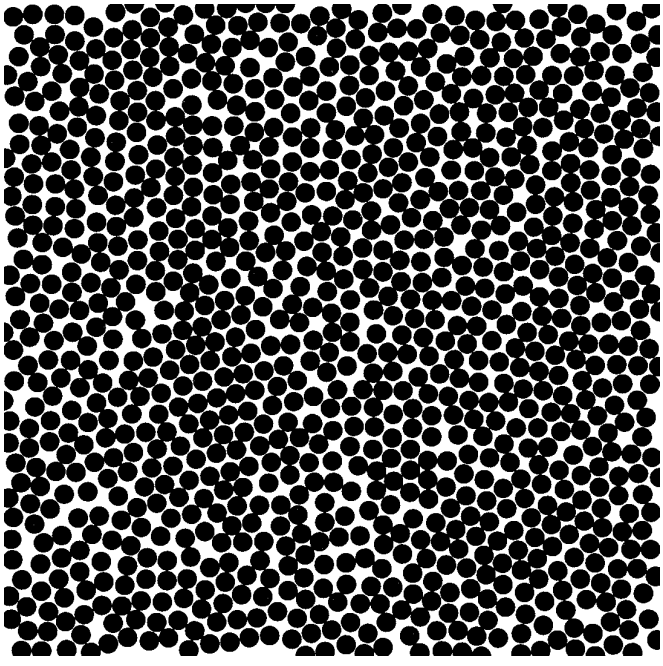

FIG. 2. A random configuration of 1024 disks in the unit cell at a disk volume fraction of 0.7.

EXAMPLE 1. A convergence study. In order to demonstrate that our method only requires a small number of degrees of freedom per disk, we consider a periodic 1024 disk configuration at volume fraction 0.7, with $\sigma_0 = 1$ and $\sigma_j = 1000$ for all inclusions (Fig. 2). With the geometry fixed, we increase the number of Fourier modes p in the discretization of the unknown density μ_j on each disk and examine the computed effective conductivity. Our results are presented in Table I, with computations carried out on an SGI workstation using the R8000 processor. The number of reflections needed in each application of the method of images was determined dynamically from the condition (24). The GMRES iteration was carried out with a tolerance of 10^{-6}.

Several observations can be made from Table I. First, five digits of accuracy are achieved using $p = 11$ terms per disk, suggesting that the constant term in the approximation (23) is very small. Second, the dense linear system with 11×1024 unknowns is solved using only 8.5 min of CPU time. Except for Helsing's adaptive integral equation method [16], we are unaware of any existing schemes for which this calculation is accessible without supercomputing

TABLE I

Convergence Study: The Effective Conductivity of the Random Composite Depicted in Fig. 2

No. terms	No. iter	CPU time	σ_{eff}
3	24	2.4214	7.68318
5	25	3.5413	7.69844
7	25	4.9437	7.67877
9	25	6.6183	7.67627
11	25	8.5126	7.67617
13	25	11.067	7.67622
15	25	13.655	7.67622
17	25	17.316	7.67622

Note. The column of Terms indicates the number of freedom (terms) used for the multipole expansion of the pseudo charge density for each disk. The column of Iter represents number of iterations needed for GMRES. CPU time is the CPU time in minutes spent to solve the boundary value problem on an SGI station with a MIPS R8000 Processor Chip. And the last column is the calculated effective conductivity.

resources. Moreover, the adaptive approach required 97 min of CPU time on a SUN SPARC10 workstation to converge to six digits with only 100 disks in the unit cell. As mentioned earlier, it is a general purpose code for inclusions of arbitrary shape and does not take advantage of the image structure we have introduced.

EXAMPLE 2. A study of system size effects. There are long-standing questions concerning system size effects in the study of random materials [42]. Various suggestions have been made in the literature about how many disks are required to simulate a truly random material [40, 6], but we are not aware of any systematic investigation of the issue, since accurate calculations in large systems have been inaccessible. We attempt to address some of these issues here by brute force: that is, by direct simulation over many instantiations of 16, 64, 256, 1024, 4096, and 16384 disk ensembles.

We will focus on the statistical properties of the effective conductivity of a random composite at volume fraction 0.5 at a contrast ratio of $\sigma_d/\sigma_0 = 1000/1$. Table II shows our results. The first column indicates the number of disks per unit cell, the second column indicates the CPU time required for a single iteration in the solution of a boundary value problem at the corresponding system size, and the third column gives the mean value and standard deviation of the effective conductivity averaged over 200 sample configurations for each system size. The last column provides an indicator of how isotropic the material is; more precisely, it is the flux in the y-direction with an electric field of unit strength applied in the x-direction. (In the random limit, the material is perfectly isotropic and the flux should be zero.)

Several facts emerge from examining the data.

1. For materials with system size 256 and below, the mean value of the effective conductivity is remarkably close to the correct value. The standard deviation however, is quite large, so that a given sample is likely to be far from the mean. In addition, the level of anisotropy can be significant.

2. As expected from a Monte Carlo process, the standard deviations for both the effective conductivity and the measure of isotropy decrease more or less linearly with the square root of the system size (the characteristic length scale).

3. Because of the incorporation of the FMM, the cost of solving the boundary value problem grows linearly with the number of disks. The largest systems considered had 11×16384 unknowns and were solved using 24 GMRES iterations in about 30 min time.

4. Beginning at system sizes of 1024, the calculation of the effective conductivity seems to be accurate to more than three digits.

Because of the last observation, we will use a system size of 1024 in our subsequent calculations, where we tabulate the effective conductivity of random composites for a wide range of volume fraction and conductivity ratio.

5.1. *Tables of Effective Properties*

Much of the work on determining the effective properties of random composites has focused on the calculation of bounds by asymptotic means. The pioneering work in this area is that of Hashin and Shtrikman [14], who established upper and lower bounds for the effective conductivity of an isotropic composite. With no additional informa-

TABLE II

System Size Effects Study: The Effective Conductivity of the Random Composites with Disk Volume Fraction at 0.5 and Disk Conductivity at $\sigma_d = 1000.0$

Size	CPU/Iter	Mean(σ_{eff}) ± S.D.	Isotropy
16	0.094	3.5587 ± 0.263	−0.002 ± 0.190
64	0.329	3.5671 ± 0.145	0.006 ± 0.097
256	1.382	3.5607 ± 0.064	−0.001 ± 0.052
1024	5.477	3.5525 ± 0.033	0.000 ± 0.027
4096	20.60	3.5519 ± 0.016	0.000 ± 0.012
16384	79.45	3.5520 ± 0.010	0.000 ± 0.009

Note. The conductivity of the matrix is $\sigma_0 = 1.0$. The first column indicates the system size (number of disks in unit cell) of the composites. The second column is the CPU time (in seconds) spent in each iteration of GMRES to solve the boundary value problem. The third column is the mean value of effective conductivity of the specified random composites and the standard deviation calculated from the sample. And the last column shows our measurements for the isotropy property of the random composites.

tion about the material, these bounds are optimal, but improvements can be made with additional information about the microstructure [3, 10, 27, 43]. Simulation methods have also been used to estimate the effective conductivity, both by Monte Carlo methods [23] and direct solution of the interface problem using small system sizes [40].

In this section, we use our method to tabulate the effective conductivity for composites consisting of random dispersions of (nonoverlapping) disks with about three digits of accuracy at volume fractions between 0.1 and 0.7 and at conductivity ratios $\sigma_d/\sigma_0 = 10.0$, 1000.0, and 10^8.

For the sake of comparison, we include the simulation results of Kim and Torquato [23] and Sangani and Yao [40] whenever available. We also provide the fourth-order Milton lower bound [28] for random materials as an approximation to the effective conductivity,

$$\sigma_L = \sigma_0 \left[\frac{\sigma_d + (1-f)\sigma_0 + f\sigma_d - (1-f)\zeta_2\lambda(\sigma_d - \sigma_0)}{\sigma_0 + f\sigma_0 + (1-f)\sigma_d - (1-f)\zeta_2\lambda(\sigma_d - \sigma_0)} \right], \tag{26}$$

where $\lambda = (\sigma_d - \sigma_0)/(\sigma_d + \sigma_0)$ and f is the disk volume fraction. This bound depends on Milton's "structural parameter" ζ_2, which is obtained numerically. We use the data of Torquato and Lado [43] for $f < 0.5$ and that of Greengard and Helsing [10] for $f \geq 0.5$. In principle, higher order bounds are possible, but their evaluation is not significantly less expensive than our current approach for calculating the effective property itself. In the figures, we also plot the effective conductivity for the square array of disks [35].

TABLE III

The Effective Conductivity of Random Composites with Disk to Matrix Conductivity Ratio $\sigma_d/\sigma_0 = 10.0$

Volume fraction	Our calculation	Four-point lower bound	Brownian simulation
0.1	1.182 ± 0.001	1.182	—
0.2	1.410 ± 0.002	1.408	1.41
0.3	1.698 ± 0.004	1.690	—
0.4	2.067 ± 0.006	2.049	2.07
0.5	2.546 ± 0.009	2.512	—
0.6	3.186 ± 0.011	3.123	3.14
0.7	4.020 ± 0.017	3.927	—

Table III and Fig. 3 concern the case $\sigma_d/\sigma_0 = 10.0$. At such low contrast, all results are in close agreement and our data simply verifies the accuracy of the previous ap-

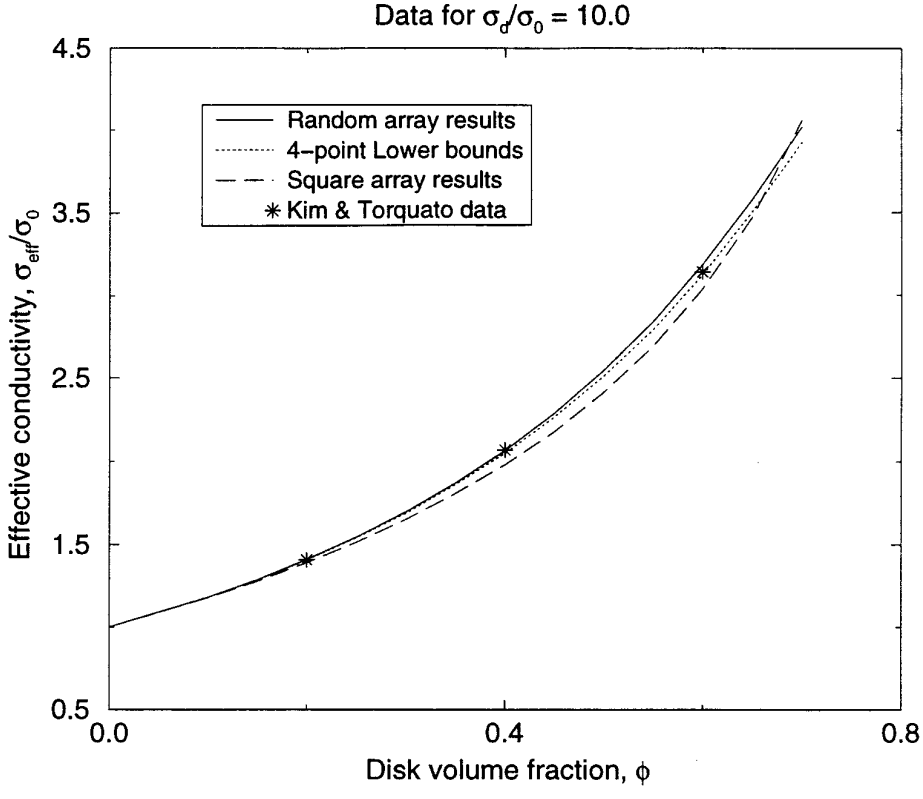

FIG. 3. Graphical display of the effective conductivity of random composites with disk to matrix conductivity ratio $\sigma_d/\sigma_0 = 10.0$.

TABLE IV

The Effective Conductivity of Random Composites with Disk to Matrix Conductivity Ratio $\sigma_d/\sigma_0 = 1000.0$

Volume fraction	Our calculation	Four-point lower bound
0.1	1.231 ± 0.001	1.229
0.2	1.541 ± 0.003	1.532
0.3	1.974 ± 0.010	1.941
0.4	2.600 ± 0.019	2.511
0.5	3.553 ± 0.033	3.338
0.6	5.114 ± 0.060	4.609
0.7	7.777 ± 0.117	6.636

TABLE V

The Effective Conductivity of Random Composites with Disk to Matrix Conductivity Ratio $\sigma_d/\sigma_0 = 10^8$

Volume fraction	Our calculation	Four-point lower bound	Brownian simulation	Sangani & Yao
0.1	1.231 ± 0.001	1.230	1.23	1.23 ± 0.002
0.2	1.543 ± 0.004	1.534	—	—
0.3	1.977 ± 0.009	1.944	1.97	1.97 ± 0.03
0.4	2.607 ± 0.018	2.517	—	—
0.5	3.571 ± 0.034	3.350	3.59	3.4 ± 0.6
0.6	5.164 ± 0.064	4.632	—	—
0.7	7.834 ± 0.119	6.684	8.29	7.8 ± 0.3

proximations. For $\sigma_d/\sigma_0 = 1000.0$, the results are shown in Table IV and Fig. 4, where significant differences can be found among the various results at high volume fractions. At the highest contrast ratio, $\sigma_d/\sigma_0 = 10^8$, our data is presented alongside previous results in Table V and Fig. 5. It is interesting to note that the results of Sangani and Yao [40] are remarkably accurate, except for the case $f = 0.5$, where the reason for the discrepancy is unclear. The simulations of Kim and Torquato [23] also gave good predictions in most cases, except that the effective conductivity was overestimated at $f = 0.7$.

An interesting phenomenon observed from the figures is that the results for square arrays consistently cross the four-point lower bound and appear likely to cross our results for random arrays at high volume fraction. Such a phenomenon has been reported earlier for the ζ_2 structural parameter [10]. It is probably due to the fact that, at high volume fractions, the random array can sample configura-

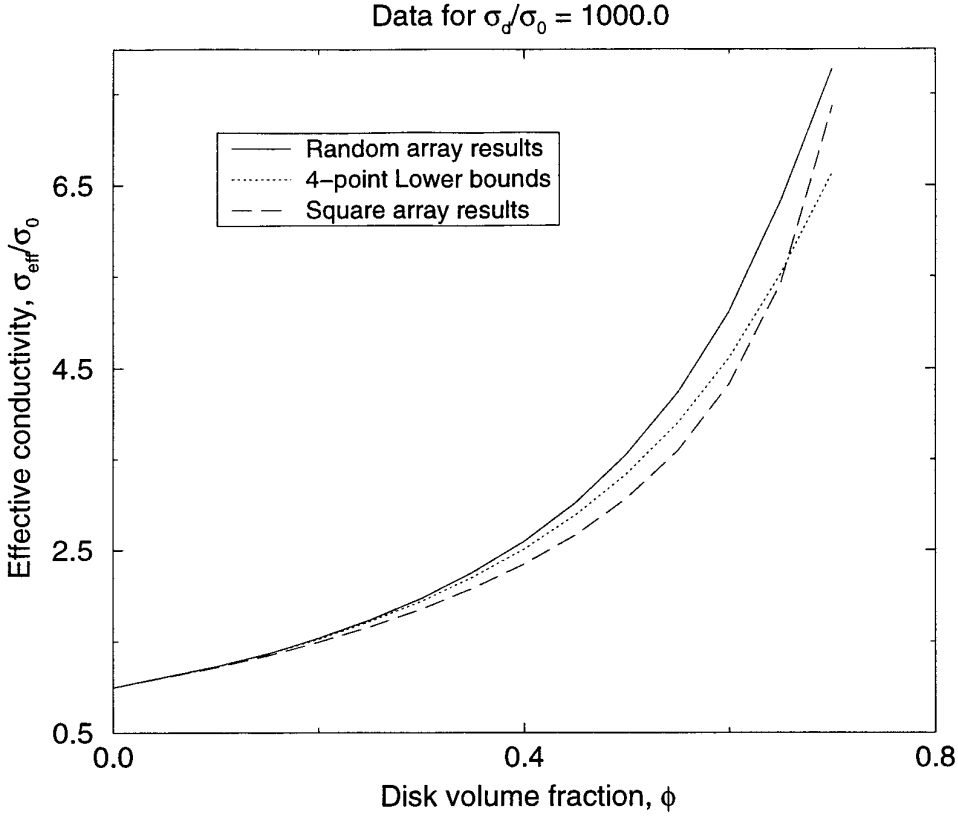

FIG. 4. Graphical display of the effective conductivity of random composites with disk to matrix conductivity ratio $\sigma_d/\sigma_0 = 1000.0$.

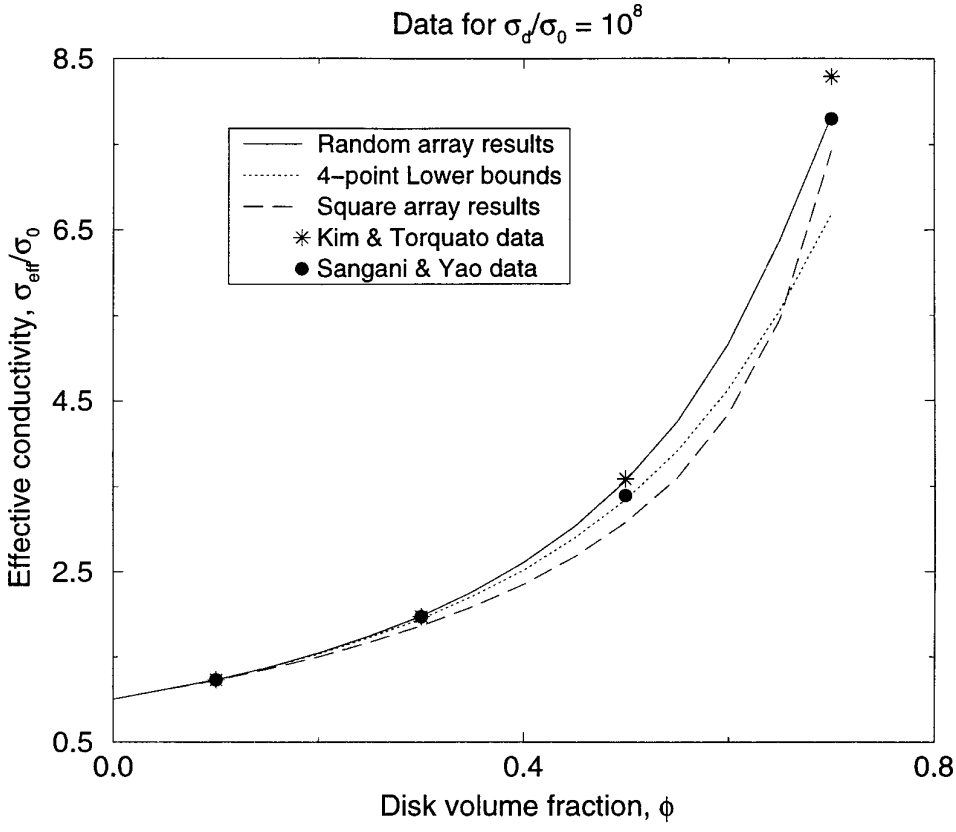

FIG. 5. Graphical display of the effective conductivity of random composites with disk to matrix conductivity ratio $\sigma_d/\sigma_0 = 10^8$.

tions closer to hexagonal close packing in structure, for which the effective conductivity is known to be lower.

5.2. *Composites with Clustered Inclusions*

To further test the capability of our method, we consider an inhomogeneous composite material, in which the inclusions are clustered (Fig. 6). Such structures can often be seen in real composites [41], and are well known to have significant effects on the transport and mechanical properties of the material under consideration, especially when clusters lead to a percolation path. Here, we consider a free-space problem in which the 1024 disks shown in Fig. 6 are embedded in a uniform background. The volume fraction of disks within the unit cell is 0.59 and the disk conductivity ratio is set to $\sigma_d/\sigma_0 = 1000/1$. To see the effect on the induced dipole moment, we carried out similar calculations for a square array of disks and for a random configuration with the same volume fraction. Our results are reported in Table VI. Note that the clustered composite requires considerably more computational effort, but still less than 20 min of CPU time. Note also that the dipole response of the random array is about 9% stronger than its square array counterpart and that the clustered array has a dipole response 13% greater than the random array.

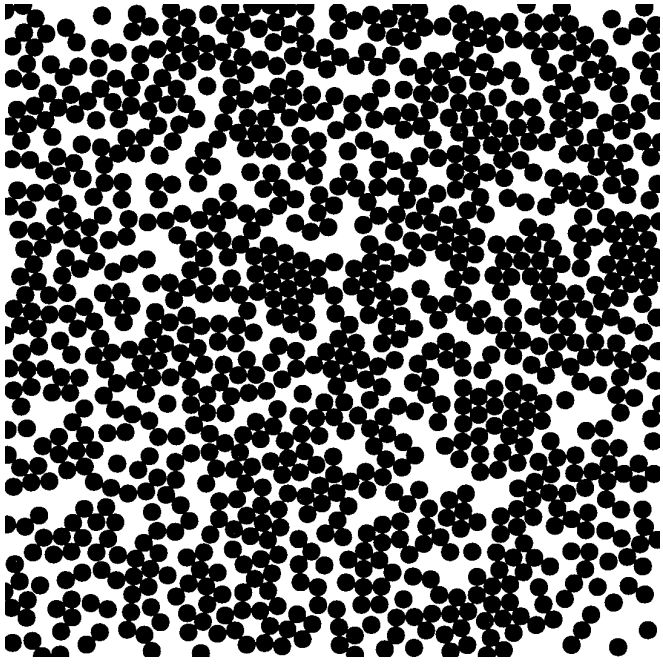

FIG. 6. An example of composite with clustered inclusions.

TABLE VI

A Comparison of the Square Array, the Random Array, and the Clustered Array in an Infinite Medium

Array type	No. terms	No. iter	CPU	Dipole
Square	5	9	24.787	(1.2654, 0.0000)
Random	11	16	124.40	(1.3810, −0.0009)
Cluster	15	72	1081.4	(1.5670, 0.0189)

Note. The first column indicates the type of disk distribution; the second column indicates the number of multipole modes required to compute the net dipole moment to the number of digits shown; and the third column indicates the number of GMRES iterations required. In the fourth column, we list the CPU times required, and in the fifth, we list the induced dipole moments.

6. DISCUSSION

We have presented a hybrid method for studying the electrostatic properties of random dispersions of disks, based on combining classical potential theory, the method of images and the fast multipole method. It is the first available method which allows for accurate numerical simulations with thousands of inclusions at trivial cost and has allowed us to construct tables of effective properties for materials over a wide range of volume fraction and conductivity ratio.

We are currently considering extensions of our scheme to the analogous three-dimensional problem (transport through random dispersions of spheres) and to problems of plane elasticity.

ACKNOWLEDGMENTS

The authors thank Professor Sal Torquato for many useful discussions and Dr. Mark Rintoul for providing the clustered configuration 6.

REFERENCES

1. G. K. Batchelor, *Ann. Rev. Fluid Mech.* **6,** 227 (1974).
2. G. K. Batchelor and R. O'Brien, *Proc. R. Soc. Lond. A* **355,** 313 (1977).
3. M. Beran, *Nuovo Cimento* **38,** 771 (1965).
4. D. J. Bergman, *Phys. Rep. C* **43,** 377 (1978).
5. C. L. Berman and L. Greengard, *J. Math. Phys.* **35,** 6036 (1994).
6. R. Bonnecaze and J. Brady, *Proc. R. Soc. Lond. A* **430,** 285 (1990).
7. H. Cheng and L. Greengard, *SIAM J. Appl. Math.*, to appear.
8. H. Cheng and S. Torquato, in preparation.
9. L. Greengard, *The Rapid Evaluation of Potential Fields in Particle Systems* (MIT Press, Cambridge, MA, 1988).
10. L. Greengard and J. Helsing, *J. Appl. Phys.* **77,** 2015 (1995).
11. L. Greengard and M. Moura, *Acta Numerica 1994* (Cambridge Univ. Press, Cambridge, 1994), p. 379.
12. L. Greengard and V. Rokhlin, *J. Comput. Phys.* **73,** 325 (1987).
13. K. Golden and G. Papanicolaou, *J. Stat. Phys.* **40,** 655 (1983).
14. Z. Hashin and S. Shtrikman, *J. Appl. Phys.* **33,** 3125 (1962).
15. J. Helsing, *Proc. R. Soc. Lond. A* **450,** 343 (1995).
16. J. Helsing, *J. Comput. Phys.* **127,** 142 (1996).
17. J. Hetherington and M. F. Thorpe, *Proc. R. Soc. Lond. A* **438,** 591 (1992).
18. E. Honein, T. Honein, and G. Herrmann, *Q. Appl. Math.* **3,** 479 (1992).
19. J. D. Jackson, *Classical Electrodynamics* (Wiley, New York, 1975).
20. M. A. Jaswon and G. T. Symm, *Integral Equation Methods in Potential Theory and Elastostatics (Academic Press, New York, 1977).*
21. J. Keller, *J. Appl. Phys.* **34,** 991 (1963).
22. J. Kellogg, *Foundations of Potential Theory,* (Dover, New York, 1953).
23. I. C. Kim and S. Torquato, *J. Appl. Phys.* **68**(8), 3892 (1990).
24. R. V. Kohn and G. W. Milton, in *Homogenization and effective moduli of materials and media,* edited by J. L. Erikson *et al.* (Springer-Verlag, New York, 1986).
25. D. Landauer, in *Electrical Transport and Optical Properties of Inhomogeneous Media,* edited by J. C. Garland and D. B. Tanner, (AIP, New York, 1978), p. 2.
26. L. D. Landau, E. M. Lifshitz, and L. P. Pitaevskii, *Electrodynamics of Continuous Media* (Pergamon, Oxford, 1984).
27. G. W. Milton, *Phys. Rev. Lett.* **46,** 542 (1981).
28. G. W. Milton, *J. Appl. Phys.* **52,** 5294 (1981).
29. G. W. Milton, *Comm. Math. Phys.* **99,** 463 (1985).
30. D. McKenzie, R. McPhedran, and G. Derrick, *Proc. R. Soc. Lond. A* **362,** 211 (1978).
31. R. McPhedran and D. McKenzie, *Proc. R. Soc. Lond. A* **359,** 45 (1978).
32. R. McPhedran and G. W. Milton, *Appl. Phys. A* **26,** 207 (1981).
33. R. McPhedran, L. Poladian, and G. W. Milton, *Proc. R. Soc. Lond. A* **415,** 185 (1988).
34. N. Metropolis, A. W. Rosenbluth, M. N. Rosenbluth, A. N. Teller, and E. Teller, *J. Chem. Phys.* **21,** 1087 (1953).
35. W. T. Perrins, R. McPhedran, and D. McKenzie, *Proc. R. Soc. Lond. A* **369,** 207 (1979).
36. Lord Rayleigh, *Phil. Mag.* **34,** 481 (1892).
37. V. Rokhlin, *J. Comput. Phys.* **60,** 187 (1985).
38. Y. Saad and M. H. Schultz, *SIAM J. Sci. Stat. Comput.* **7,** 856 (1986).
39. A. S. Sangani and A. Acrivos, *Proc. R. Soc. Lond. A* **386,** 263 (1982).
40. A. S. Sangani and C. Yao, *Phys. Fluids* **31,** 2426 (1988).
41. S. Torquato, *Appl. Mech. Rev.* **44**(2), 37 (1991).
42. S. Torquato, *Appl. Mech. Rev.* **47**(1), s29 (1994).
43. S. Torquato and F. Lado, *Proc. R. Soc. Lond. A* **438,** 591 (1988).
44. J. R. Willis, *Adv. Appl. Mech.* **21,** 1 (1981).